Magnetic impurity bands in Ga_{x−1}Mn_{x}S: Towards understanding the anomalous spin-glass transition

M. C. Massey, I. Manuel, P. S. Edwards, D. Parker, T. M. Pekarek, and J. T. Haraldsen

Phys. Rev. B **98**, 155206 — Published 29 October 2018

DOI: 10.1103/PhysRevB.98.155206

Magnetic impurity bands in $Ga_{x-1}Mn_xS$: Towards understanding the anomalous spin-glass transition

M.C. Massey, I. Manuel, P.S. Edwards, D. Parker, T.M. Pekarek, and J.T. Haraldsen
Department of Physics, University of North Florida, Jacksonville, FL 32224, USA
(Dated: October 10, 2018)

We report on the magnetic and electronic properties of single crystalline $Ga_{0.91}Mn_{0.09}S$, which is a quasi-two-dimensional diluted magnetic semiconductor. Through an analysis of magnetization data, we show the existence of an anomalously high spin-glass transition temperature at 11.2 K. Using density functional theory (DFT), we characterize the properties contributing to the spin-glass transition through an examination of the electronic and magnetic properties for $Ga_{1-x}Mn_xS$ with x varying from 0.00 to 0.18 by randomly substituting Mn atoms into the gallium (Ga) lattice sites. We show that the presence of magnetic atoms produces impurity bands in the electronic structure, where an analysis of the density of states shows an increase in magnetic impurity bands at the Fermi level that lowers the semiconducting gap and is consistent with diluted magnetic semiconductors. Furthermore, this indicates that the spin-glass transition in $Ga_{0.91}Mn_{0.09}S$ is similar to other DMS materials, where the primary mechanism is likely through magnetic exchange. However, the increased electron density in the system with Mn doping could explain the anomalously higher spin-glass transition temperature in $Ga_{0.91}Mn_{0.09}S$. In comparison with the substantially lower transition temperatures in related II-VI based systems (i.e., $Zn_{1-x}Mn_xTe$), the high transition temperature is typically associated with more metallic spin-glass systems that interact through RKKY exchange, which leads to the conclusion that there may be a combination of interactions occurring in these systems. Further measurements on the other substitution percentages will hopefully clarify these interactions.

I. INTRODUCTION

Early spin-glass materials such as $Cu_{1-x}Mn_x$ and $Au_{1-x}Fe_x$ consist of a metal (e.g., Au, Cu, or Ag) with transition metal ions (e.g., Fe, Mn, or Cr) embedded throughout the host metal[1]. The magnetic properties introduced by the transition metal impurities created promising opportunities to investigate transport properties and the interaction of magnetic moments in metals and dilute alloys[2]. These materials undergo a long-range magnetic transition from the normal state above the critical temperature T_c to the spin-glass state below T_c. This long-range magnetic ordering arises from the *s-d* exchange interaction between the conducting electrons of the metal host and the substituted magnetic ions. The mechanism for the spin-glass transition was based on the Ruderman, Kittel, Kasuya, and Yosida (RKKY) exchange mediated by conduction electrons. In the RKKY exchange, spin polarization is induced in conduction electrons which leads to indirect coupling between magnetic ions[3–6].

In contrast, insulating spin-glass materials derived from chalcogenides (e.g., $Eu_xSr_{1-x}S$, $Eu_xSr_{1-x}As_3$, and $Eu_xSr_{1-x}Te$)[1] lack readily available conduction electron states. Without conduction electrons, the RKKY exchange cannot exist, and so it was not considered possible that these materials could undergo a true spin-glass transition. Instead, the coupling between magnetic ions in insulating materials is dominated by superexchange[7]. This exchange channel results from *sp-d* hybridization where neighboring magnetic ions are coupled through orbital interactions between magnetic and non-magnetic ions[8]. $Eu_xSr_{1-x}S$ is a particularly short-range spin-glass

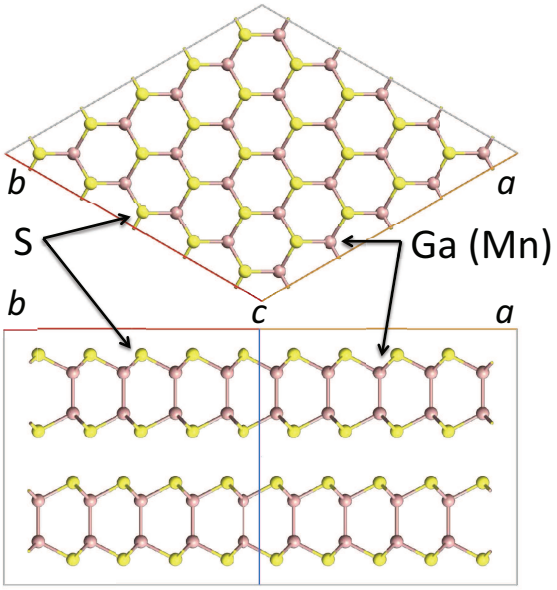

FIG. 1: Crystal structure for $Ga_{1-x}Mn_xS$ lattice in *ab*-plane (top panel) and along the *c*-direction (bottom panel).

with a strong neighbor and next-nearest neighbor spin interactions. The insulating $Eu_xSr_{1-x}S$ system transitions from spin-glass behavior to a superparamagnetic state for concentrations below the percolation threshold $x_p = 0.13$[1,9]. This case provides strong evidence against a model in which independent clusters of spins describe a spin-glass[9]. With the acceptance of superexchange as the dominant mechanism for interactions between magnetic ions in insulating systems, $Eu_{1-x}Sr_xS$ and other insulat-

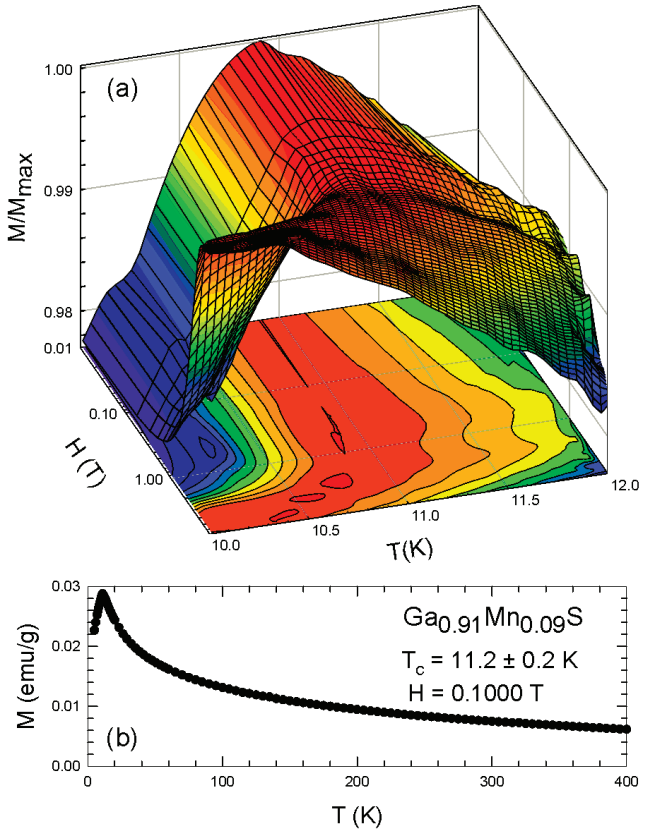

FIG. 2: (a) Normalized magnetization versus temperature and field for $Ga_{0.91}Mn_{0.09}S$. Note the log scale on the H(T) axis. (b) Magnetization versus temperature for the system taken in a 0.1 T field. The critical temperature T_c at 11.2 K is just above the 10.9 K cusp at low fields. Above the T_c, the spin-glass exhibits paramagnetism. Below the T_c, the magnetization exhibits behavior that suggests that a spin-glass transition is taking place. The 0.1 T magnetization data was previously published in Ref. [35].

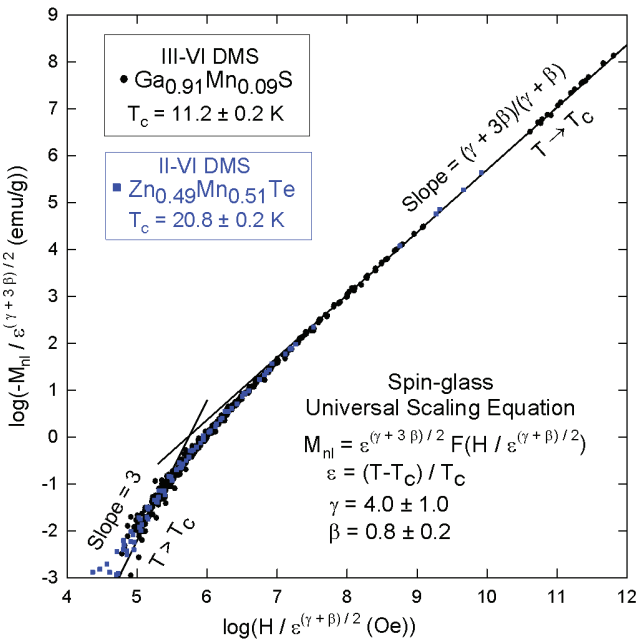

FIG. 3: The nonlinear magnetization data analyzed according to a universal scaling model for $Ga_{0.91}Mn_{0.09}S$ and $Zn_{0.49}Mn_{0.51}Te$. There is an excellent overlap following the same universal scaling function over the entire range. The universal scaling relation was used to confirm that $Ga_{0.91}Mn_{0.09}S$ alongside $Zn_{0.49}Mn_{0.51}Te$ undergoes a true spin-glass transition. This analysis was previously published in Ref. [35].

ing materials were established as a new class of spin-glass systems.

Transition-metal chalcogenide materials have become a hot topic in the field of condensed matter physics due to their semiconducting properties and wide range of configurations and elemental variance[10–13]. These are materials that are sulfur (S), selenium (Se), and tellurium (Te) based, where the tunability of these materials makes them ideal for technological applications as well as provides a playground for the examination of complex interactions[11].

The chalcogenide materials can have many different configurations depending on the crystal symmetry around the metal atoms. The most popular are the dichalcogenide materials (MX_2)[12,14–18]. These two-dimensional (2D) materials have hexagonal structures that have a sandwich like configuration (X-M-X), where M is typically a transition metal. This configuration typically leads to semiconducting materials with either a direct band gap (monolayer) or indirect band gap (bulk)[19,20].

Additionally, there are monochalcogenide configurations. Typically, the transition metal monochalcogenide materials are bulk materials ranging from cubic to hexagonal structures[13,21–23]. However, the M_2X_2 configuration of the MX chalcogenides mixes the 2D structure of dichalcogenide materials with the stoichiometry of the monochalcogenide materials. Similar to the dichalcogenides, the 2D MX chalcogenides have two metal atoms in the center (X-M-M-X), where the M and X bond form a honeycomb lattice in the *ab*-plane and quasi-2D layers that are connected through van der Waals interactions (illustrated in Fig. 1.)

The 2D MX chalcogenide materials are typically produced using M = Ga and In, which leads to insulating materials such as GaS[24,25]. However, the doping of the Ga and In sites with transition-metal elements has lead to interesting physical phenomena such as long range magnetic order and spin interactions[26–35].

Gallium sulfide (GaS) and other III-VI doped and un-doped semiconductors are well known for exhibiting remarkable optical properties including a large nonlinear coefficient, THz generation and detection, high-temperature operation, high damage threshold, and a wide transparency range[36–45]. Doping with Te[40,41], Cr[39], Ag[36], and Er[38] strengthens GaSe. Doping with In significantly enhances the physical properties and strength-

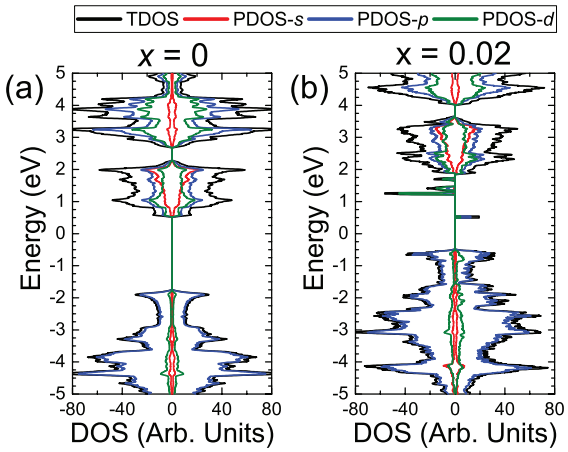

FIG. 4: Calculated total and partial electronic density of states for $Ga_{1-x}Mn_xS$ with $x = 0$ and 0.02, where the TDOS (black), PDOS-*s* (red), PDOS-*p* (blue), PDOS-*d* (green). The positive and negative DOS denote the spin up and down channels, respectively. To guide the eye, the contribution lines are total, *p*, *d*, and *s* from the outside in at the -4.0 eV level.

ens the crystals enough to allow optical surfaces to be cut and polished along additional directions. Surprisingly, doping with In does not diminish the useful properties of GaSe but actually enhances the non-linear optical properties[39–45].

The incorporation of a transition metal element raises intriguing possibilities for coupling the magnetic properties of the transition metal ion with the host III-VI semiconductor leading to optical or electrical transport effects. Specifically, the *sp-d* exchange coupling in related materials can sometimes have dramatic physical consequences such as giant Faraday rotation, bound magnetic polarons, or induced metal to insulator transitions[46,47].

In this study, we present magnetization measurements on $Ga_{0.91}Mn_{0.09}S$, where an analysis of this data shows the presence of a spin-glass transition at 11.2 K, which is too high to be associated with the standard superexchange spin-glass systems, but too low for the metallic RKKY spin-glasses. Therefore, to further understand the nature of this transition, we performed density functional calculations on Mn-doped supercells of GaS. Starting with the undoped GaS system, we effectively dope the supercells through substitution of Mn atoms into random Ga sites and then calculate the electronic and magnetic properties. We find that a distinct magnetic moment is produced on the Mn sites, which is governed by a standard antiferromagnetic superexchange. An analysis of the electronic density of states indicates the production of transition-metal impurity bands near the Fermi level, which lowers the semi-conducting gap and allows for orbital interactions between the Mn and S sites. The lowering of the semiconducting gap may explain the higher transition temperature in this material.

II. EXPERIMENTAL AND COMPUTATIONAL METHODOLOGY

A 0.0160 g single crystalline $Ga_{0.91}Mn_{0.09}S$ sample was grown by the vertical Bridgman method with a nominal concentration of x = 0.05. Magnetization measurements were performed using a Quantum Design MPMS XL7 superconducting quantum interference device (SQUID) magnetometer at temperatures between 1.8 and 400 K in fields up to 7 T. The 0.1 T magnetization data and spin-glass analysis was previously published in Ref. [35]. A Curie-Weiss fit at high temperatures gave a concentration of x = 0.091. A concentration of x = 0.089 was obtained from a comparison of the magnetization values over a range of fields up to 7 T and temperatures above the cusp up to 400 K with the values obtained from a reference sample whose actual concentration was determined by both a Curie-Weiss analysis and atomic absorption spectroscopy (AAS). We, therefore, take the actual concentration of our sample to be x = 0.09. Measurements for the nonlinear scaling analysis were made for fields between 0 and 1 T. An undoped GaS crystal was measured to determine the value of the diamagnetic signal (-3.7 x 10^{-7} emu/g G) due to the semiconductor host GaS, which was subtracted from the data.

Computational analysis was performed using Density Functional Theory (DFT) provided by Atomistix Toolkit[48,49]. Starting with the well-documented GaS structure[24,50], we simulated a 100-atom supercell (shown in Fig. 1), which restricts concentrations to even amounts. To help reduce computational time, we considered only one quasi-2D layer and randomly substituted Ga atoms with Mn atoms to mimic experimental doping levels. Test simulations on the multiple layers with and without van der Waals interactions showed no major difference.

All structures were energy minimized and geometry optimized to a tolerance of 0.01 eV/$\AA$ using a Limited-Memory Broyden-Fletcher-Goldfarb-Shanno (LBFGS) method. The DFT calculations were performed using a Spin-Polarized General Gradient Approximation (SGGA) with Perdew, Burke, and Ernzerhof (PBE) functionals with a self-consistent tolerance of 10^{-5} Hartrees with a 10x10x1 *k*-point sampling and standard electron temperature of 300K. Calculations of the energy gap for the mother compound of GaS were compared to previously published calculations[50] and found to be consistent around 3 eV.

For analysis, we determined the electronic density of states, electron density, magnetic moment, optical spectrum, and total energy for doping levels of x = 0 to 0.18 by 0.02. Furthermore, we determined the electronic properties for both the ferromagnetic (FM) and antiferromagnetic (AFM) magnetic configurations.

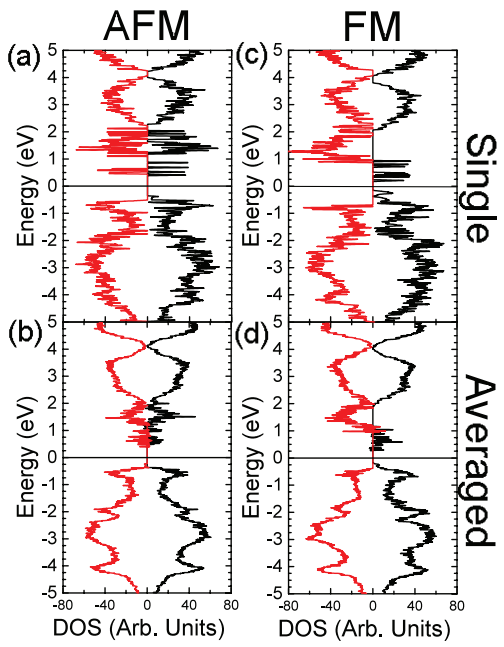

FIG. 5: Comparison of the antiferromagnetic and ferromagnetic density of states for a single (a) and (c) and configuration averaged (b) and (d) $x = 0.08$ substitution. The positive and negative DOS denote the spin up and down channels, respectively.

III. THE SPIN-GLASS TRANSITION

Figure 2(a) shows the temperature and field dependencies of the normalized magnetization data from 10 to 12 K and 0.01 to 7 T, where the cusp in the M(T) data occurs around 10.9 K for $Ga_{0.91}Mn_{0.09}S$. As expected for a spin-glass transition, this maximum in the magnetization occurs at a slightly lower temperature than the 11.2 K spin-glass transition temperature. Figure 2(b) shows the magnetization versus temperature for $Ga_{0.91}Mn_{0.09}S$ in a 0.1 T field. From 400 K down to 15 K the magnetization is featureless following a standard Curie-Weiss temperature dependence for a paramagnet.

A detailed scaling analysis of the nonlinear magnetization M_{nl} for $Ga_{0.91}Mn_{0.09}S$ was previously published in Ref. [35] and is shown in Fig. 3 for data taken between 11.2 and 13.0 K in several set fields between 0.0130 and 0.1000 T. The key feature is that the data all collapse onto a single universal scaling function $F(H/\epsilon^{(\gamma+\beta)/2})$ given by

$$M_{nl}(\epsilon, H) = ^{(\gamma+3\beta)/2} F(H/\epsilon^{(\gamma+\beta)/2}), \qquad (1)$$

over several orders of magnitude along both axes. This fit is shown in Fig. 3 by the solid circles. Here H is the applied field, ϵ = (T - T_c) / T_c is the reduced temperature, and γ and β are critical exponents. Additionally, the data approaches a slope of $(\gamma + 3\beta)/(\gamma + \beta)$ for temperatures near T_c and approaches a slope of 3 for T > T_c as expected for a spin-glass transition. This nonlinear scaling analysis is the key test for a true spin-glass transition[1]. We, therefore, conclude that there is a true transition from the paramagnetic to the spin-glass state at 11.2 K for $Ga_{0.91}Mn_{0.09}S$.

Also shown in Fig. 3 is the nonlinear scaling analysis for $Zn_{1-x}Mn_xTe$ (solid squares). The data for both $Ga_{0.91}Mn_{0.09}S$ and $Zn_{1-x}Mn_xTe$ collapse onto the same universal scaling function over many orders of magnitude along both axes. Both approach the same asymptotic limits and both have the same values for the critical exponents. However, despite both systems being based on semiconducting hosts, their spin-glass transition temperatures are dramatically different versus Mn concentration.

From this magnetization analysis, we see an anomalously high spin-glass transition temperature for $Ga_{0.91}Mn_{0.09}S$ that more closely resembles metallic spin-glass systems, which suggests that something unusual could be occurring, perhaps involving the presence of conducting electrons in $Ga_{0.91}Mn_{0.09}S$ at low temperatures. However, the T_c for $Ga_{0.91}Mn_{0.09}S$ is still well below the values for the metallic spin-glass systems indicating that any conduction electrons would be playing a much smaller role than in the metallic systems. To address this intriguing result, we conducted detailed DFT calculations to explore the role of the electronic states in $Ga_{0.91}Mn_{0.09}S$.

IV. DENSITY FUNCTIONAL CALCULATIONS

To understand the electronic and magnetic properties in $Ga_{0.91}Mn_{0.09}S$, we performed DFT calculations to examine the electronic density of states, electron density, magnetic moment, and optical spectrum. The goal is to gain insight into the possible origin for the anomalous spin-glass transition temperature observed in the bulk magnetic measurements[35].

Through an examination of the Mulliken population, we determine that the magnetic moment on the Mn atoms is about 4.0 μ_B, which indicates that the oxidation state of the Mn atoms is 2+ (due to only three unpaired electrons), if we introduce an on-site potential to the Mn 3*d* electrons, then the oxidation is shifted toward the Mn^{3+} state with little shifting of the impurity bands, which is also shown in recent calculations on the fully doped M_2X_2 materials[52].

In Fig. 4 we show the total and partial electronic density of states (DOS) for the FM and AFM configurations of $Ga_{1-x}Mn_xS$ for $x = 0$ and 0.02 concentrations. Here, the total density of states (TDOS) are in black and partial density (PDOS) is broken into the orbital contributions from the *s*- (red), *p*- (blue), and *d*- (green) orbitals. The solid and dashed lines denote the spin up and down channels, respectively. From the data, it is clear that the presence of Mn impurities into the GaS structure pro-

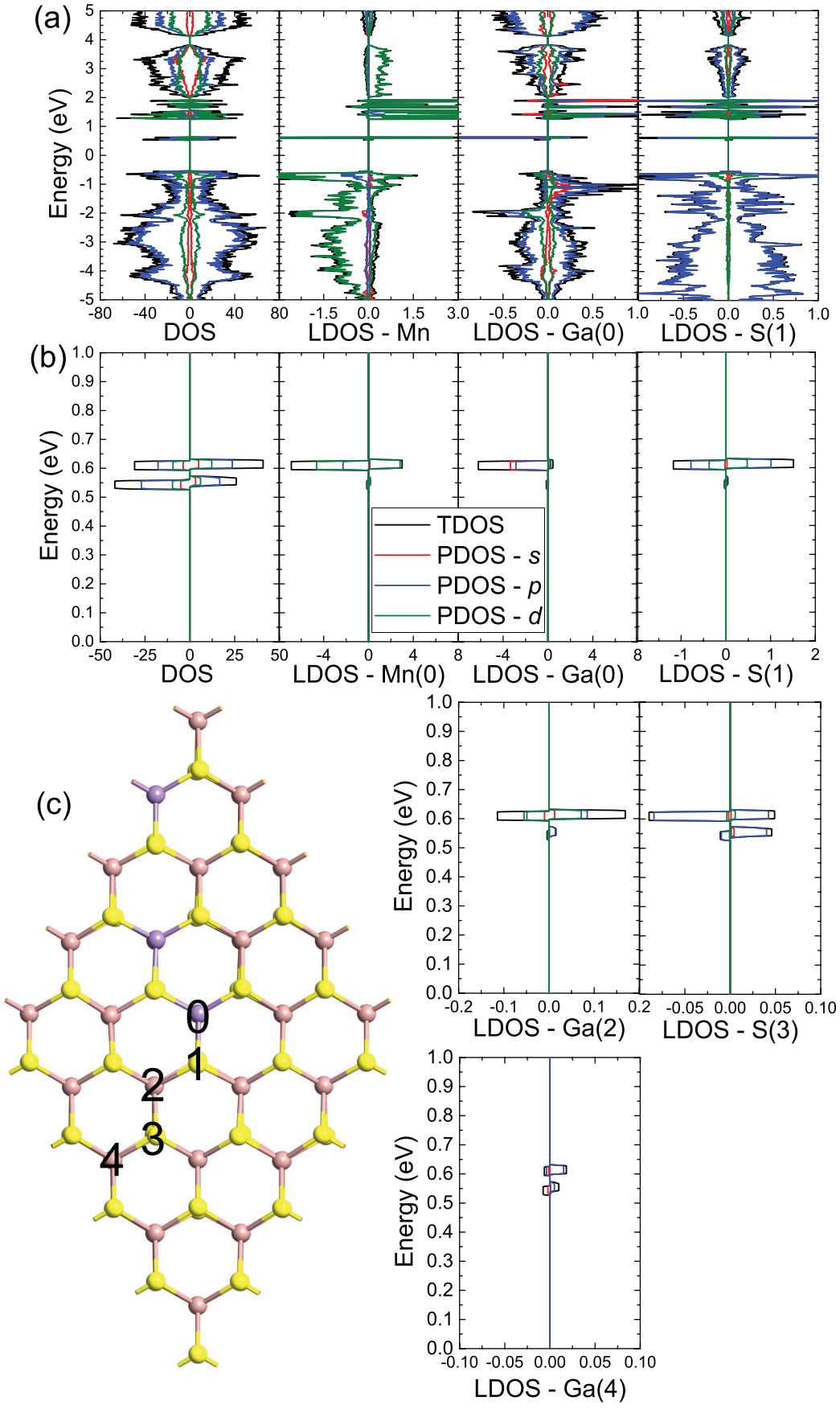

FIG. 6: (a) Total, partial, and local density states for the $x = 0.08$ concentration. (b) Zoomed in view of the impurity state at 0.6 eV.The positive and negative DOS denote the spin up and down channels, respectively.(c) An illustration of the spatial positions for the atom examined for the local density of states.

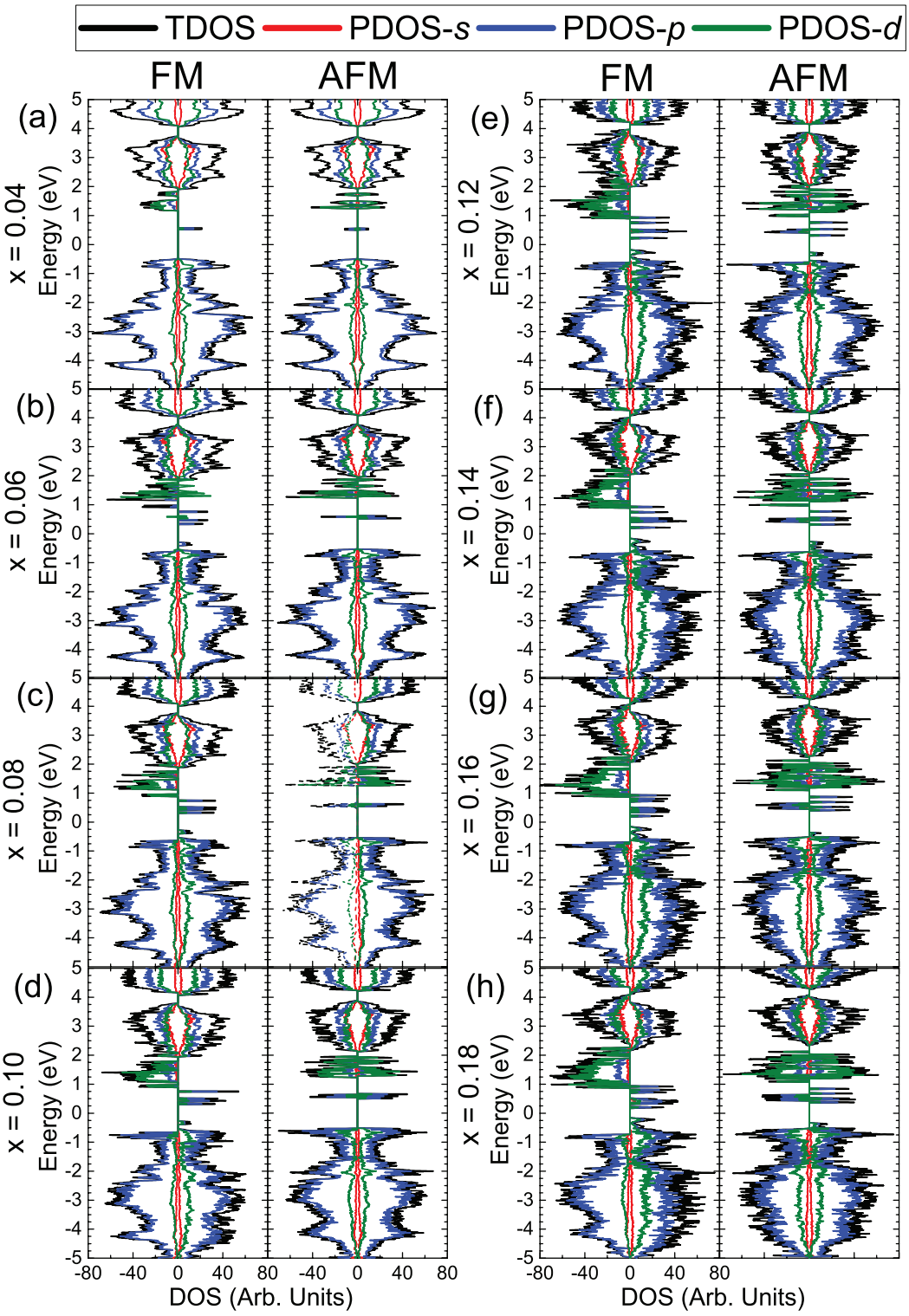

FIG. 7: Calculated total and partial electronic density of states for $Ga_{1-x}Mn_xS$ with $x = 0.04$ to 0.18 by 0.02, where the TDOS (black), PDOS-s (red), PDOS-p (blue), PDOS-d (green). The positive and negative DOS denote the spin up and down channels, respectively. To guide the eye, the contribution lines are total, p, d, and s from the outside in at the -4.0 eV level.

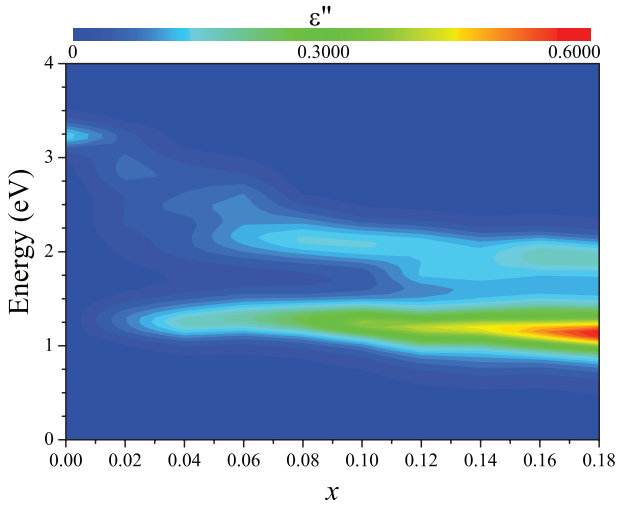

FIG. 8: Calculated imaginary component of the dielectric function as a function of energy and percent substitution.

duces an impurity band near the Fermi level. The DOS for GaS (Fig. 4(a)) clearly shows an insulating gap of about 3.2 eV, which is consistent with the experimental value[50]. However, as shown in Fig. 4(b), the presence of only 2% doping of Mn produces an impurity band near the Fermi surface, which begins to lower the gap energy.

To clarify the nature of the impurity bands, Figure 6 examines the total, partial, and local DOS for the $x = 0.08$ concentration focusing on the Mn and Ga atoms, where the lower panels of the figure zooms into the impurity bands to examine the orbital contributions and clearly shows that the band come from the Mn impurities. Since the $x = 0.08$ concentration has more Mn atoms, the number of impurity bands increases. Furthermore, this seems to indicate the potential for *pd*-orbital hybridization from the Mn atoms coupling to *sp*-orbitals from the Ga. This is due to the shifting of electrons in the Mn-Ga bonds as the system is doped. Furthermore, by examining the LDOS of multiple atoms in the unit cell, it is clear that the presence of the Mn atoms induces a this impurity state in the surrounding atoms, which extends to multiple atoms away from the magnetic impurity (shown in Fig. 6(c)). A similar state has been observed in $Ga_{1-x}Mn_xAs$[51].

To examine the evolution of the impurity states further, we calculated the electronic and magnetic properties for various concentrations. Figure 7 details the total and partial electronic density of states (DOS) for the FM and AFM configurations of $x = 0.04$ to 0.18 (Fig. 7). Here, we did not employ the averaging since it is clear it will simply widen the impurity bands.

The issue with concentrations larger than $x = 0.02$ in these simulations are that there could be multiple spatial and spin configurations. Therefore, one has to average over these configurations. In Fig. 5, we show the single and averaged total DOS for the AFM and FM configurations for the $x = 0.08$ concentration, since this is closest to the experimental concentration. This data shows that the averaging effect over multiple configurations widens and "blurs" the impurity bands near the Fermi level, which is typically expected.

TABLE I: Total Energies (in eV) for the Antiferromagnetic and Ferromagnetic Configurations.

x	E_{AFM}	E_{FM}	ΔE
0.04	-22167.504	-22167.504	0.000
0.06	-22723.508	-22723.270	-0.238
0.08	-23279.365	-23279.124	-0.240
0.10	-23835.193	-23834.954	-0.240
0.12	-24390.919	-24390.650	-0.269
0.14	-24946.732	-24946.456	-0.275
0.16	-25502.807	-25502.300	-0.507
0.18	-26058.590	-26058.069	-0.520

From the simulations, Table I shows an analysis of the total energy for the FM and AFM configurations where the AFM arrangement is the dominate ground state, which is consistent with the magnetization measurements that exhibits AFM behavior determined by the Curie-Weiss extrapolation[35]. The change in energy is given by E_{AFM} - E_{FM}, where a positive value indicates a FM ground state and negative is AFM. It should be noted that these energies are for the single configurations and not averaged over multiple magnetic configurations. The $x = 0.04$ concentration is degenerate because the spins are far enough away of each other not to correlate. Therefore, the AFM and FM are equally probable.

As more Mn atoms are introduced into the supercell, the number of Mn impurity bands near the Fermi level is increased (shown in Fig. 7). As the increased presence of impurity bands begins to fill in the energy gap, the system shifts from an insulator to a diluted magnetic semiconducting state. Recent calculations on MnS have indicated that the system will become completely metallic as the system is fully doped[52]. Therefore, indicating that there may be a threshold or increase in the transition temperature of the spin-glass state as one increases doping.

To illustrate the shifting of the gap energy, we calculated the imaginary part of the dielectric function (Fig. 8). Here, there is a definite red shift in energy from the insulation gap of 3.2 eV towards the semi-conducting gap of about 1 eV, which provides a precise prediction for experimental optical measurements on these types of systems. It should be noted that this gap was determined by single calculations. When averaged over multiple configurations, the widening of the impurity bands may lead to a smaller gap as more metallic-like pathways are populated.

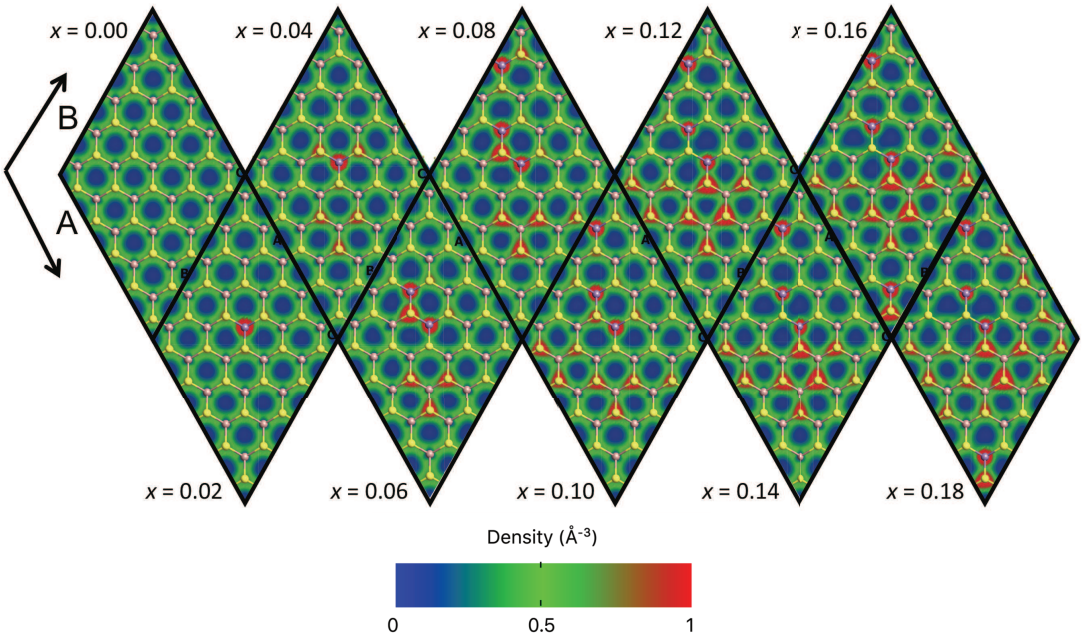

FIG. 9: Calculated electron density for $Ga_{1-x}Mn_xS$ with $x = 0 \rightarrow 0.18$ by 0.02. The color scale goes from 0 (blue) to 1 (red) $Å^{-3}$, where red indicates increased density.

V. DISCUSSION

The magnetization data from Ref. [35] and shown above clearly indicates the presence of a spin-glass transition and antiferromagnetic ordering. Furthermore, the density functional simulations demonstrate that $Ga_{0.91}Mn_{0.09}S$ is a diluted magnetic semiconductor, which is not mutually exclusive to spin-glass order.

Figure 10 shows the corresponding spin-glass transition temperatures for known metallic, insulating, and semiconducting materials. From this plot, metallic spin-glass materials (red triangles) have relatively high T_c's at deficient doping concentrations due to the ability of spin coupling through RKKY interactions. Insulating (green x) and semiconducting materials (blue circles, squares, and diamonds) have much lower T_c's since the spin interactions occur through orbital superexchange.

The II-VI diluted magnetic semiconductors (II-VI DMS) ($A^{II}_{1-x}M_xB^{VI}$) are based on an $A^{II}B^{VI}$ semiconductor host with a fraction x of magnetic ion M substituting at the group II lattice site. As expected for a semiconductor system at low temperatures, where the carriers are frozen out, the mechanism for interaction between magnetic ions in a II-VI DMS spin-glass is due to superexchange as is observed in insulating materials[60]. Since semiconductors have a lower electronic gap energy, their T_c can dramatically increase as the chemical potential is enhanced with doping.

When we plot the spin-glass transition temperature of 11.2 K for $Ga_{0.91}Mn_{0.09}S$ in Fig. 10, as shown by the black star, we find that the transition temperature is substantially higher than what we would expect for a semiconducting system. As is seen in Fig. 10, the II-VI DMS systems have transition temperatures close to those observed for the insulating spin-glass systems for x < 0.2. In the case of both the insulating and II-VI systems, the spin-glass transitions are believed to arise from superexchange rather than due to conduction electrons via the RKKY interaction. This dilemma provides the exciting possibility of having a system that combines the two regimes.

A key difference between metallic and insulating spin-glass systems is how the doping concentration affects the spin-glass transition temperature. As seen in Fig. 10, the metallic spin-glass transition occurs at high temperatures for low doping concentrations (e.g., $Cu_{1-x}Mn_x$[55–57] and $Au_{1-x}Fe_x$[58,59]). In contrast, the insulating spin-glass systems (e.g., $Eu_xSr_{1-x}S$[9]) maintain a low spin-glass transition temperature even at high doping concentrations. The II-VI DMS (e.g., $Zn_{1-x}Mn_xTe$, $Cd_{1-x}Mn_xTe$[53,54], and $Cd_{1-x}Mn_xSe$[54]) have low transition temperatures for doping concentrations below 0.2 similar to the insulating spin-glass systems. Interestingly, the spin-glass transition temperature T_c increases faster for concentrations above 0.2. To our knowledge, this faster rise in T_c is not fully understood.

Through an analysis of the DOS, it is clear that the $Ga_{1-x}Mn_xS$ system is insulating and non-magnetic at x = 0. However, upon doping with Mn, the system gains a magnetic moment that induces impurity bands at the Fermi level. These impurities provide the basis for the shifting chemical potential that pushes the insulating state to a semiconducting state.

Furthermore, by comparing the total energies of the

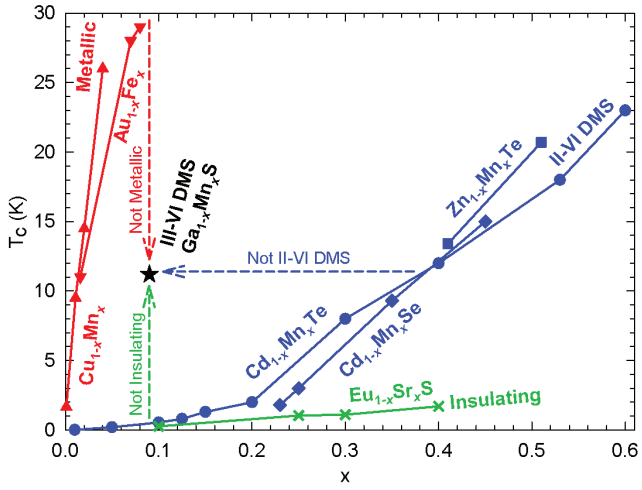

FIG. 10: Spin-glass transition temperature T_c versus concentration x for various spin-glass materials. The metallic spin-glass systems (e.g. $Cu_{1-x}Mn_x$[55–57] and $Au_{1-x}Fe_x$[58,59]) have high values of T_c for small values of x. In contrast, T_c remains below 2K for insulating materials (e.g. $Eu_{1-x}Sr_x$[9]) for a wide range of x. The II-VI DMS systems (e.g. $Cd_{1-x}Mn_xTe$[53,54]) have T_c values similar to the insulating spin-glass systems for $x < 0.2$. For the same value of x, the III-VI DMS $Ga_{0.91}Mn_{0.09}S$[35] system is an order of magnitude larger than the insulating and II-VI DMS systems and about a factor of three smaller than the metallic systems. The lines are a guide to the eye.

FM and AFM states, we find that the AFM configuration is dominant, which indicates that superexchange is the main contributor to the interaction between spins. This interaction is further confirmed by the partial DOS that shows the possibility of *sp-d* hybridization in the impurity bands. However, the system does not produce a metallic signature in the DOS, which means there is no avenue for the presence of an RKKY interaction like that observed in the metallic materials. However, Fig. 9 shows the electron density for each calculated system. Here, the red indicates an increase in electron density with the presence of Mn atoms. Although, it should be noted that there is a distinct increase in electron density on the nearest neighbor sulfur atoms, which is likely responsible to the increased communication between the Mn atoms in the spin glass phase. This is further supported by the presence of the impurity bands in sulfur and gallium LDOS (shown in Fig. 6).

From the electron density and density of states, the placement of $Ga_{0.91}Mn_{0.09}S$ in Fig. 10 starts to become more evident. In combination with the DOS crossover in the impurities, this indicates a pathway towards the metallic region. Recently, it was shown that in the case of a complete substitution of Mn atoms, the system becomes metallic[52]. From this analysis, it appears that the increased doping of Mn atoms into the Ga sites leads to a semi-conducting materials that exhibits some semi-metallic characteristics, which provides a possible avenue for metallic behavior, even though the system is not metallic. Therefore, While $Ga_{0.91}Mn_{0.09}S$ is a diluted magnetic semiconductor, the spin glass T_c is about ten times higher than other semiconductors at that doping concentration but does not have the free carriers of a metal to increase its T_c further.

Previous studies on the hole doping of Ga_2X_2 structures have shown the possibility of Lifshitz transitions due to change in the Fermi surface topology[50], which could provide a mechanism for the increase in T_c with transition-metal substitution. Figure 9 shows the increasing percolation of electron density from the addition of Mn atoms. While this is not surprising, the increase in electron density on the sulfur sites around the Mn sites indicates a network of orbital overlap. As more Mn is added to the system, we would expect that the transition temperature would increase towards the metallic regime in Fig. 10, since the system appears to become more metallic with substitution[52]. Further systematic experimental studies of intermediate concentrations will hopefully clarify this state.

VI. CONCLUSION

In conclusion, we show the presence of a sharp spin-glass transition at 11.2 K in the diluted magnetic semiconductor $Ga_{0.91}Mn_{0.09}S$, which provides an exciting crossover between the standard metallic spin-glasses that interact through RKKY and the insulating spin-glasses that interact through superexchange. Using density functional theory, we show that the increase of Mn into the Ga sites of GaS produces impurity bands that shift the gap energy from insulating to semiconducting. The presence of an antiferromagnetic ground state and lack of metallicity at the Fermi level suggests that the magnetic moments interact through a standard superexchange mechanism. However, increased electron density due to the presence of the Mn atoms could provide a mechanism for spin-glass state and may explain the higher transition temperature, even though the system is non-metallic and does not interact through RKKY.

The importance of this manuscript stems from the identification of this anomalous spin-glass transition and the work towards understanding it. These calculations show that the presence of impurity bands near the Fermi level and increased electron density and density of states could provide a semi-metallic state that allows for communication between spin states and may produce a spin glass state. Therefore, further systematic measurements on doping levels in $Ga_{1-x}Mn_xS$ are being planned and may provide a clearer understanding of the nature of this spin-glass transition.

Acknowledgements

I.M. and J.T.H recognize support by the Institute for Materials Science at Los Alamos National Laboratory. T.M.P. acknowledges support from the UNF Terry Presidential Professorship, the Florida Space Grant Consortium, and by the National Science Foundation (NSF) Grant Nos. DMR-16-26332 and DMR-14-29428.

[1] K. H. Fisher and J. A. Hertz, Spin Glasses (University Press, Cambridge, 1991).
[2] V. Cannela and J. A. Mydosh, Magnetic Ordering in Gold-Iron Alloys, Phys. Rev. B **6**, 4220 (1972).
[3] M. A. Ruderman and C. Kittel, Indirect Exchange Coupling of Nuclear Magnetic Moments by Conduction Electrons, Phys. Rev. **96**, 99 (1954).
[4] T. Kasuya, A Theory of Metallic Ferro- and Antiferromagnetism on Zener's Model, Prog. Theor. Phys. **16**, 45 (1956).
[5] K. Yosida, Magnetic Properties of Cu-Mn Alloys, Phys. Rev. **106**, 893 (1957).
[6] T. Dietl, A. Haury, and Y. Merle dAubigne, Free carrier-induced ferromagnetism in structures of diluted magnetic semiconductors, Phys. Rev. B **55**, R3347 (1997).
[7] K. Binder and A. P. Young, Spin Glasses: Experimental facts, theoretical concepts, and open questions. Phys. Rev. B 58, 801 (1986).
[8] P. W. Anderson, New Approach to the Theory of Superexchange Interactions, Phys. Rev. 115, 2 (1959).
[9] H. Maletta and W. Felsh, Insulating spin-glass system $Eu_xSr_{1x}S$, Phys. Rev. B 20, 1245 (1979).
[10] D. J. Vaughan, J. R. Craig, Mineral Chemistry of Metal Sulfides Cambridge University Press, Cambridge: 1978.
[11] J. Zhou, J. Lin, X. Huang, Y. Zhou, Y. Chen, J. Xia, H. Wang, Y. Xie, H. Yu, J. Lei, D. Wu, F. Liu, Q. Fu, Q. Zeng, C.-H. Hsu, C. Yang, L. Lu, T. Yu, Z. Shen, H. Lin, B.I. Yakobson, Q. Liu, K. Suenaga, G. Liu, and Z. Liu, A library of atomically thin metal chalcogenides, Nature **556** 355 (2018).
[12] Q.H. Wang, K. Kalantar-Zadeh, A. Kis, J. N. Coleman, and M.S. Strano, Electronics and optoelectronics of two-dimensional transition metal dichalcogenides, Nature Nanotechnology **7**, 699 (2012).
[13] H. Wang and X. Qian, Two-dimensional multiferroics in monolayer group IV monochalcogenides, 2D materials **4**, 015042 (2017).
[14] L. F. Mattheiss, Band Structures of Transition-Metal-Dichalcogenide Layer Compounds, Phys. Rev. B **8**, 3719 (1973).
[15] A.A. Al-Hilli and B.L. Evans, The preparation and properties of transition metal dichalcogenide single crystals, Journal of Crystal Growth **15**, 93 (1972).
[16] W. S. Yun, S. W. Han, S. C. Hong, I. G. Kim, and J. D. Lee, Thickness and strain effects on electronic structures of transition metal dichalcogenides: 2H-MX_2 semiconductors (M = Mo, W; X = S, Se, Te), Phys. Rev. B **85**, 033305 (2012).
[17] A. Ramasubramaniam, D. Naveh, and E. Towe,Tunable band gaps in bilayer transition-metal dichalcogenides, Phys. Rev. B **84**, 205325 (2011).
[18] C. Ataca, H. ahin, and S. Ciraci, Stable, Single-Layer MX_2 Transition-Metal Oxides and Dichalcogenides in a Honeycomb-Like Structure, J. Phys. Chem. C, **116**, 8983 (2012).
[19] A. Splendiani, L. Sun, Y. Zhang, T. Li, J. Kim, C. Y. Chim, G. Galli, F. Wang, Emerging Photoluminescence in Monolayer MoS_2. Nano Letters **10** 1271 (2010).
[20] K.F. Mak, C. Lee, J. Hone, J. Shan, T. F. Heinz, Atomically Thin MoS_2: A New Direct-Gap Semiconductor. Physical Review Letters **105** 136805 (2010).
[21] N. C. Fernelius, Properties of gallium selenide single crystal, Prog. Cryst. Growth Charact. Mater. **28**, 275 (1994).
[22] A. Segura, J. Bouvier, M. V. Andrés, F. J. Manjón, and V. Muñoz, Strong optical nonlinearities in gallium and indium selenides related to inter-valence-band transitions induced by light pulses, Phys. Rev. B **56**, 4075 (1997).
[23] S. Nüsse, P. H. Bolivar, H. Kurz, V. Klimov, and F. Levy, Carrier cooling and exciton formation in GaSe, Phys. Rev. B **56**, 4578 (1997).
[24] H. Hahn and G. Frank, Über die Kristallstruktur des GaS, Zeitschrift fuer Anorganische und Allgemeine Chemie **278**, 348 (1955).
[25] M. R. Lazell, P. O'Brien, D. J. Otway, and J.-H. Park. Deposition of Thin Films of Gallium Sulfide from a Novel Single-Source Precursor, Ga $(S_2CNMeHex)_3$, by Low-Pressure Metal Organic Chemical Vapor Deposition. *Chemistry of materials* **11**, 3430 (1999).
[26] S. Shigetomi, T. Ikari, and H. Nakashima, Impurity levels in layer semiconductor *p*-GaSe doped with Mn, J. Appl. Phys. **76**, 310 (1994).
[27] L. T. Vinh, M. Eddrief, J. E. Mahan, A. Vantomme, J. H. Song, and M. A. Nicolet, The van der Waals epitaxial growth of GaSe on Si(111), J. Appl. Phys. **81**, 7289 (1997).
[28] S. Nüsse, P. H. Bolivar, H. Kurz, F. Levy, A. Chevy, and O. Lang, Femtosecond coherent polariton dynamics in the layered III-VI semiconductor InSe, Phys. Rev. B **55**, 4620 (1997).
[29] D. Errandonea, A. Segura, J. F. Sánchez-Royo, V. Muoz, P. Grima, A. Chevy, and C. Ulrich, Investigation of conduction-band structure, electron-scattering mechanisms, and phase transitions in indium selenide by means of transport measurements under pressure, Phys. Rev. B **55**, 16217 (1997).
[30] V. N. Katerinchuk and M. Z. Kovalyuk, Gallium telluride heterojunctions, Tech. Phys. Lett. **25**, 54 (1999).
[31] J. Z. Wan, J. L. Brebner, and R. Leonelli, Possibility of coherent light emission from excitons in crystalline GaTe, Phys. Rev. B **53**, 15413 (1996).
[32] Pekarek, T. M., M. Duffy, J. Garner, B. C. Crooker, I. Miotkowski, and A. K. Ramdas. Magnetic measurements on the layered III-VI diluted magnetic semiconductor $Ga_{1-x}Mn_xS$. *Journal of Applied Physics* **87**, no. 9 (2000): 6448-6450.
[33] Pekarek, T. M., C. L. Fuller, J. Garner, B. C. Crooker, I. Miotkowski, and A. K. Ramdas. Magnetic measurements on the layered III-VI diluted magnetic semiconductor $Ga_{1-x}Fe_xSe$. *Journal of Applied Physics* **89**, no. 11 (2001): 7030-7032.
[34] Pekarek, T. M., D. J. Arenas, I. Miotkowski, and

A. K. Ramdas. "Magnetic and transport measurements on the layered III-VI diluted magnetic semiconductor $In_{1x}Mn_xSe$." *Journal of applied physics* **97**, no. 10 (2005): 10M106.

[35] T.M. Pekarek, E.M. Watson, J. Garner, P.M. Shand, I. Miotkowski, A. K. Ramdas, J. Appl. Phys. 107, Spin-glass ordering in the layered III-VI diluted magnetic semiconductor $Ga_{1x}Mn_xS$, 09E136 (2010).

[36] J.J. Xie, J. Guo, L.M. Zhang, D.J. Li, G.L. Yang, F. Chen, K. Jiang, M.E. Evdokimov, M.M. Nazarov, U.M. Andreev, G.V. Lanskii, K.A. Kokh, A.E. Kokh, and V.A. Svetlichnyi, Optical properties of non-linear crystal grown from the melt GaSe-$AgGaSe_2$, Optics Comm. 287, 145-149 (2012).

[37] W. Shi, Y.J. Ding, N. Fernelius, and K. Vodopyanov, Efficient, tunable, and coherent 0.18-5.27-THz source based on GaSe crystal, Optics Lett. 27, 1454-1456 (2002).

[38] C.W. Chen, Y.K. Hsu, J.Y. Huang, and C.C. Chang, Generation properties of coherent infrared radiation in the optical absorption region of GaSe crystal, Opt. Express 14, 10636 (2006).

[39] G. Xu, G. Sun, Y.J. Ding, I.B. Zotova, K.C. Mmandal, A. Mertiri, G. Pabst, and N. Fernelius, Investigation of symmetries of second-order nonlear susceptibility tensor of GaSe crystals in THz domain, Optics Comm. 284, 2027-2030 (2011).

[40] Z. Rak, S.D. Mahanti, K.C. Mandal, and N.C. Fernelius, Doping dependence of electronic and mechanical properties of $GaSe_{1-x}Te_x$, and $Ga_{1-x}In_xSe$ from first pricniples, Phys. Rev. B 82, 155203 (2010).

[41] K.C. Mandal, S.H. Kang, M. Choi, J. Chen, X.C. Zhang, J.M. Schleicher, A. Achmuttenmaer, and N.C. Fernelius, III-VI Chalcogenide Semiconductor Crystals for Broadband Tunable THz Sources and Sensors, IEEE J. of Selected Topics in Quantum Electronics 14, 284 (2008).

[42] V.G. Voevodin, O.V. Voevodina, S.A. Bereznaya, Z.V. Korotchenko, A.N. Morozov, S.Y. Sarkisov, N.C. Fernelius, and J.T. Goldstein, Large single crystals of gallium selenide: growing, doping by In and characterization, Optics Materials 26, 495-499 (2004).

[43] Z.S. Feng, Z.H. Kang, F.G. Wu, J.Y. Gao, Y. Jiang, H.Z. Zhang, Y.M. Andreev, G.V. Lanskii, V.V. Atuchin, and T.A. Gavrilova, SHG in doped GaSe:In crystals, Opt. Express 16, 9978 (2008).

[44] D.R. Suhre, N.B. Singh, V. Balakrishna, N.C. Fernelius, and F.K. Hopkins, Improved crystal quality and harmonic generation in GaSe doped with indium, Opt. Lett. 22, 775 (1997).

[45] N.B. Singh, D.R. Suhre, W. Rosch, R. Meyer, M. Marable, N.C. Fernelius, F.K. Hopkins, D.E. Zelmon, and R. Narayanan, J. Cryst. Growth 198-199, Modified GaSe crystals for mid-IR applications, 588 (1999).

[46] See, for example, in Semiconductors and Semimetals, edited by J. K. Furdyna and J. Kossut (Academic, Boston, 1988), Vol. 25.

[47] J. K. Furdyna, Diluted magnetic semiconductors, J. Appl. Phys. 64, R29, (1988).

[48] Atomistix ToolKit version 13.8, QuantumWise A/S (www.quantumwise.com)

[49] Soler, J. M. et al. The SIESTA method for ab initio order-N materials simulation. *J. Phys.: Condens. Matter* **14**, 2745 (2002).

[50] V. Z´lyomi, N. D. Drummond, and V. I. Falk,Band structure and optical transitions in atomic layers of hexagonal gallium chalcogenides, Phys. Rev. B 87, 195403 (2013).

[51] K. Z. Milowska and M. Wierzbowska, Hole sp^3-character and delocalization in (Ga, Mn)As revised with pSIC and MLWF approaches Newly found spin-unpolarized gap states of s-type below 1% of Mn, Chem. Phys. **430**, 7-12 (2014).

[52] T. La Martina, J.-X. Zhu, A.V. Balatsky, and J.T. Haraldsen, Dirac nodes and magnetic order in M_2X_2 transition-metal chalcogenides, Physica Status Solidi - RRL 1800181 (2018).

[53] M. A. Novak, O. G. Symko, and D. J. Zheng, Spin-glass behavior of $Cd_{1x}Mn_xTe$ below the nearestneighbor percolation limit, J. Appl. Phys. 57, 3418 (1985).

[54] S. B. Oseroff, Magnetic susceptibility and EPR measurements in concentrated spin-glasses: $Cd_{1x}Mn_xTe$ and $Cd_{1x}Mn_xSe$, Phys. Rev. B 25, 6584 (1982).

[55] P. Gibbs, T. M. Harders, and J. H. Smith, The magnetic phase diagram of CuMn, J. Phys. F: Met. Phys. 15, 213 (1985).

[56] L. Lundgren, P. Svedlindh, P. Nordblad, and O. Beckman, Dynamics of the Relaxation-Time Spectrum in a CuMn Spin-Glass, Phys. Rev. Lett. 51, 911 (1983).

[57] S. Nagata, P. H. Keesom, and H. R. Harrison, Low-dc-field susceptibility of CuMn spin-glass Phys. Rev. B 19, 1633 (1979).

[58] L. E. Wenger and P. H. Keesom, Magnetic ordering of $Au_{0.92}Fe_{0.08}$: A calorimetric investigation, Phys. Rev. B 11, 3497 (1975).

[59] J. S. Senoussi, New information on the spin-glass state of AuFe from transport measurements, Phys. F: Met. Phys. 10, 2491 (1980).

[60] B. E. Larson, K. C. Hass, H. Ehrenreich, and A. E. Carlsson, Theory of exchange interactions and chemical trends in diluted magnetic semiconductors, Phys. Rev. B 37, 4137 (1988).